REVIEW ARTICLE

Variational data assimilation for deriving global climate analyses from GNSS radio occultation data

A. Löscher · G. Kirchengast

Abstract A comprehensive global navigation satellite system (GNSS) based radio occultation (RO) data set is available for meteorology and climate applications since the start of GNSS RO measurements aboard the CHAllenging Mini-satellite Payload (CHAMP) satellite in February 2001. Global coverage, all-weather capability, long-term stability and accuracy not only makes this innovative use of GNSS signals a valuable supplement to the data set assimilated into numerical weather prediction (NWP) systems but also an excellent candidate for global climate monitoring. We present a 3D variational data assimilation (3D-Var) scheme developed to derive consistent global analysis fields of temperature, specific humidity, and surface pressure from GNSS RO data. The system is based on the assimilation of RO data within 6 h time windows into European Centre for Medium-Range Weather Forecasts (ECMWF) short-term (24 h, 30 h) forecasts, to derive climatologic monthly mean fields. July 2003 was used as a test-bed for assessing the system's performance. The results show good agreement with climatologies derived from RO data only and recent NWP impact studies. These findings are encouraging for future developments to apply the approach for longer term climatologic analyses, validation of other data sets, and atmospheric variability studies.

Introduction

Since there is evidence that human activities influence the Earth's climate (IPCC 2007), the accurate determination of the atmospheric state using all suitable and available data is mandatory to monitor and project its evolution over decades to come (Leroy et al. 2006).

Global Navigation Satellite System (GNSS) radio occultation (RO) is a technique featuring an unique combination of global coverage, all weather capability, high accuracy and long-term stability suggesting it is a near-ideal method for long-term monitoring of atmospheric and climate variability and change (Anthes et al. 2000; Kirchengast et al. 2000; Leroy and North 2000; Steiner et al. 2001, 2007; Gobiet et al. 2005, 2007; Borsche et al. 2007; Foelsche et al. 2007). RO observations also exhibit a high vertical resolution (<1 km) and an accuracy of individual profiles of better than 1 K in the upper troposphere/lower stratosphere (UTLS) region (Steiner et al. 2006; Gobiet et al. 2007).

The long-term stability property distinguishes RO from most other satellite observational techniques allowing the compilation of data series spanning decades without common inter-calibration problems (Thorne et al. 2005) from

A. Löscher
European Space Agency/European Space Research and Technology Centre (ESA/ESTEC), Noordwijk, The Netherlands

A. Löscher · G. Kirchengast
Wegener Center for Climate and Global Change (WegCenter), Institute for Geophysics, Astrophysics, and Meteorology (IGAM), University of Graz, Graz, Austria

A. Löscher (✉)
EOP-SF, ESTEC, P.O. Box 299,
2200, AG, Noordwijk, The Netherlands
e-mail: Armin.Loescher@esa.int; armin.loescher@uni-graz.at

different RO receiver types and platforms. Examples include the CHAllenging Mini-satellite Payload (CHAMP) which provides data since 2001 (Wickert et al. 2001), the Constellation Observing System for Meteorology Ionosphere and Climate (FORMOSAT-3/COSMIC) providing data since mid 2006 (Rocken et al. 2000; Wu et al. 2005), and the Meteorological Operational Satellite (MetOp) series GNSS receiver for atmospheric sounding (GRAS). This first operational GNSS RO mission will provide data from 2007 to 2020 (Loiselet et al. 2000; Luntama et al. 2007).

CHAMP has been providing almost continuously about 200 RO events daily since late 2001 from which about 150–170 quality approved atmospheric profiles can be derived (Wickert et al. 2004). Based on these data, NWP impact studies have been conducted at the UK Met Office and the European Centre for Medium-Range Weather Forecasts (ECMWF), showing a positive effect on forecasts and analyses (Healy et al. 2005; Healy and Thépaut 2006). Multi-annual climatologies have been derived, showing that sampling errors caused by the sparse data flow of one single GNSS RO receiver, as in the case of CHAMP, still allow for accurate seasonal mean temperature climatologies to resolve large horizontal scales >1,000 km as well as monthly zonal means (Foelsche et al. 2006, 2007; Pirscher et al. 2007).

As to climate analysis, the use of reanalysis data such as ERA40 (Kållberg et al. 2004) or NCEP-NCAR Reanalysis (Kistler et al. 2001) for trend studies, proofed to be problematic since it has been found difficult to reliably isolate trends of the climate system (Bengtsson et al. 2004). The problems mainly originate from changes of the observation systems.

In this study, we explore an optimal way to combine (higher density) model field information with (sparse) RO data for climate studies. We introduce a demonstration implementation of the three-dimensional variational data assimilation (3D-Var) technique to generate statistically optimal and self-consistent fields by combining RO observations with short-term NWP forecasts. The analyses obtained at about 300 km horizontal resolution are providing complementary information to coarse grids of climatological bins (bin size scale >1,000 km) derived from RO data only, e.g., Foelsche et al. (2006, 2007). In an optimal case the procedure allows a better characterization of biases and accuracy by taking uncertainties of both RO data and background fields into account.

Methodology and setup of the 3D-Var system

The 3D-Var is an iterative optimization technique combining data of different sources in a statistically optimal

way. Detailed introductions are given by Bouttier and Courtier (1999) and Kalnay (2003).

3D-Var

The 3D-Var optimization problem, set to find a minimum of a cost function $J(\mathbf{x})$, can be expressed as follows:

$$\mathbf{x}_a = \text{Arg min } J, \tag{1}$$

$$J(\mathbf{x}) = J_b(\mathbf{x}) + J_o(\mathbf{x}), \tag{2}$$

$$J(\mathbf{x}) = \frac{1}{2}\Big\{ (\mathbf{x} - \mathbf{x}_b)^T \mathbf{B}^{-1} (\mathbf{x} - \mathbf{x}_b) \\ + (\mathbf{y} - H(\mathbf{x}))^T \mathbf{R}^{-1} (\mathbf{y} - H(\mathbf{x})) \Big\}, \tag{3}$$

$$\nabla J_{\mathbf{xa}} = \mathbf{B}^{-1}(\mathbf{x}_a - \mathbf{x}_b) + \mathbf{H}^T \mathbf{R}^{-1}[H(\mathbf{x}_a) - \mathbf{y}] = 0, \tag{4}$$

where $\mathbf{x}$ represents the atmospheric state vector containing the so-called control variables, $\mathbf{x}_a$ the updated state vector at convergence (i.e., the resulting analysis), $\mathbf{y}$ the observation vector, $J_b(\mathbf{x})$ and $J_o(\mathbf{x})$ are the background x and observation cost functions respectively. The minimization problem can be solved either in terms of full fields, $\mathbf{x}$, or in terms of increments, $\delta\mathbf{x}$,

$$\delta\mathbf{x} = \mathbf{x} - \mathbf{x}_b, \tag{5}$$

$$J(\delta\mathbf{x}) = \frac{1}{2}\Big[\delta\mathbf{x}^T \mathbf{B}^{-1} \delta\mathbf{x} + (\mathbf{H}\delta\mathbf{x} - \mathbf{d})^T \mathbf{R}^{-1} (\mathbf{H}\delta\mathbf{x} - \mathbf{d}) \Big], \tag{6}$$

$$\mathbf{d} = \mathbf{y} - H(\mathbf{x}_b), \tag{7}$$

$$\nabla J = \mathbf{B}^{-1}\delta\mathbf{x} + \mathbf{H}^T \mathbf{R}^{-1} \mathbf{H}\delta\mathbf{x} - \mathbf{H}^T \mathbf{R}^{-1}\mathbf{d}, \tag{8}$$

where the analysis is found by adding the final increment $\delta\mathbf{x}_a$ to the first guess,

$$\mathbf{x}_a = \mathbf{x}_b + \delta\mathbf{x}_a. \tag{9}$$

$\delta\mathbf{x}_a$ is found by minimizing the cost function (6) using the cost function gradient (8) and a suitable optimization algorithm. The differences $H(\mathbf{x}) - H(\mathbf{x}_b)$ are written as $\mathbf{H}\delta\mathbf{x}$ using a linear approximation, where $H(\mathbf{x})$ is the potentially non-linear observation operator and $\mathbf{H}$ is the linear approximation (tangent linear operator) of H. Furthermore, $\mathbf{H}^T$ is the adjoint operator, and $\mathbf{R}$ and $\mathbf{B}$ are the observation and background error covariance matrices, respectively. To reduce the numerical cost and practically enable global analyses in terms of CPU time, control space transformations including preconditioning (Zupanski 1993; Kozo 1997) can be performed.

Specific implementation

We did choose an incremental 3D-Var formulation, based on Equations (5)–(9), using control space transformations

and recursive filters; the dimensions of the grid are flexible.

Assimilation system setup

The demonstration ("test-bed") setup is based on a general circulation model (GCM) compliant Gaussian grid corresponding to T42L60, i.e., 64 latitudes × 128 longitudes and 60 vertical model levels (sigma levels of ECMWF fields). The horizontal resolution matches with the along-ray-integrating character of the RO technique (the majority of atmospheric bending occurs within a horizontal interval of 200–300 km centered on the tangent point), e.g., Kursinski et al. (1997), and allows for a numerically efficient implementation. The 24 h of a day are divided into 6 h time windows around 00, 06, 12 and 18 UTC to perform separate assimilation runs using the appropriate background fields and set of observations (±3 h around the analysis time). Monthly means are derived by averaging the analyses of the individual time windows.

We use temperature, specific humidity, and surface pressure as the control variables (i.e., atmospheric state fields). Cross-correlations between them are assumed to be small enough to be neglected, giving block-diagonal background covariance matrices; horizontal and vertical correlations are assumed to be separable. The cost function is minimized by using an iterative minimization algorithm (L-BFGS-B) based on the Broyden–Fletcher–Goldfarb–Shanno method (Zhu et al. 1995; Nocedal 1996).

Control space transformations

Minimization of the cost function of a state vector $\mathbf{x}$ with n degrees of freedom is numerically expensive. The solution which we chose is to perform the minimization in a control variable space $\mathbf{v}$ (Barker et al. 2003), which reduces the number of required minimization steps since the problem becomes better posed. Appropriately implemented, the background error covariance matrix approximately satisfies $\mathbf{B}_c = \mathbf{I}$ in control space, where $\mathbf{I}$ denotes the identity matrix; hence the problem is effectively preconditioned. In terms of increments, the control variable transform can be written as

$$\delta\mathbf{x} = \mathbf{U}\mathbf{v}. \tag{10}$$

The transformation

$$\mathbf{v} = \mathbf{U}^{-1}\delta\mathbf{x} \tag{11}$$

serves to break down the atmospheric state $\mathbf{x}$ into uncorrelated but physically realistic error modes, which can be penalized in J_b according to their estimated error

magnitude (Skamarock et al. 2005; Barker et al. 2004). The control variable transform as expressed in Eq. (10) in fact consists of a sequence of operations,

$$\delta\mathbf{x} = \mathbf{U}_v\mathbf{U}_h\mathbf{v}, \tag{12}$$

where the subscript h denotes the horizontal and v the vertical part of the transform. Respective transformations proceed from control to model space but are reversed in the adjoint calculations. The associated $\mathbf{B}$ in its expanded form is written as:

$$\mathbf{B} = \mathbf{U}_v\mathbf{U}_h\mathbf{U}_v^T\mathbf{U}_h^T. \tag{13}$$

Vertical control variable transform

The vertical transform projects control variables from model levels onto the weighted eigenvectors of the vertical component of the background error covariance matrix. This covariance matrix $\mathbf{B}_v$ is given as a $k \times k$ positive-definite symmetric matrix, where k is equal to the number of vertical levels. That allows us to perform an eigenvalue decomposition. Thus a transformation $\mathbf{U}_v\mathbf{v}$ between variables $\delta\mathbf{x}(k)$ on model levels and their projection onto vertical modes m can be defined by

$$\mathbf{B}_v = \mathbf{U}_v\mathbf{U}_v^T. \tag{14}$$

This allows us to derive

$$J_b = \frac{1}{2}\sum_m \mathbf{v}_v^2(m) \tag{15}$$

for the background cost function, and

$$\nabla J_b = \mathbf{v}_v \tag{16}$$

for the background gradient, respectively. This leads to significant CPU time savings in calculating the background cost function via (15) and the background gradient via (16).

Horizontal control variable transform

The horizontal control variable transform is based on the identity (cf. 13),

$$\mathbf{B}_h = \mathbf{U}_h\mathbf{U}_h^T, \tag{17}$$

which is formally analogous to the vertical control variable transform (14), but realized for the sake of numerical efficiency by scaled recursive filters (RF). The RF is defined through an initial function A_j at grid points j, where $1 \le j \le J$. A single pass of the RF consists of an initial smoothing from *left* to *right*,

$$B_j = \alpha B_{j-1} + (1 - \alpha)A_j \text{ for } j = 1\ldots J. \tag{18}$$

followed by another pass from *right* to *left*,

$$C_j = \alpha C_{j+1} + (1 - \alpha)B_j \text{ for } j = J \ldots 1. \qquad (19)$$

Applying the RF in each direction ensures zero phase change. A 1-pass filter is defined as a single application of Equations (18) and (19), whilst an N-pass RF is defined by N sequential applications of these equations. The symbol α denotes the filter coefficients, which are derived such that the filter output matches analytical functions; for the limit $N \to \infty$, the output of the RF tends to be Gaussian. To ensure correct zero-distance behavior (i.e., correct value at the grid point itself), a scaling factor S is defined by taking the inverse of the zero-distance response of a one dimensional N-pass RF to a delta function. A two-dimensional RF results by a second perpendicular application of a one-dimensional RF and the use of S^2 as scaling factor. Only $N/2$ passes are performed when applying the RF in forward mode, the other $N/2$ passes are performed by the adjoint transform as indicated in Equation (17), (the adjoint corresponds to the transpose). Details concerning RF's and the matching with analytical functions are given by Lorenc (1992) and Hayden and Lorenc (1995). We used a six pass filter ($N = 6$), where the coefficients α were calculated to approximate the horizontal error structures of the control variables (on error characteristics see "RO data and background data" below). To solve the "boundary problem" (that there is by construction no transfer of information from point 1 to point J and vice versa), the filter is applied a second time with a shifted grid arrangement (Löscher et al. 2006). To illustrate this, Fig. 1 (top) represents a latitude or longitude band divided into four equal segments.

To be able to transfer information from A to D and vice versa, the filter procedure is applied a second time to a shifted arrangement of segments as illustrated in Fig. 1 (bottom). After the second filtering process, the original order of the boxes is reconstructed using the two middle segments from both runs, ensuring a smooth transition between the boxes A and D.

Observation operator

The observation operator ($H(\mathbf{x})$ in "3D-Var" above) consists of interpolation routines and the forward model to convert interpolated state vector quantities to the observed

A	B	C	D
C	D	A	B
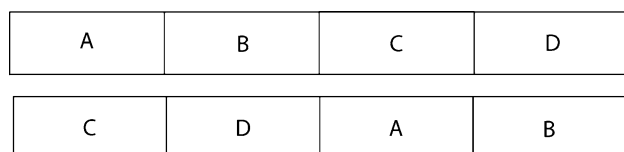
Fig. 1 Segments along one latitude or longitude band in original order and in shifted arrangement

quantity (refractivity cf. "RO data and background data"). A simplification of the Smith-Weintraub refractivity formula is used as forward model (e.g. Kursinski et al. 1997),

$$N = k_1 \frac{p_A}{T} + k_3 \frac{e}{T^2}, \qquad (20)$$

where N denotes the refractivity, T the temperature, p_A pressure (dry term), e the partial pressure of water vapor (wet term), and $k_1 = 77.6$ K hPa^{-1}, $k_3 = 373 \times 10^3$ K^2 hPa^{-1} are empirical constants. In order to calculate the corresponding gradients, the adjoint of the observation operator is used, which was derived by using TAPENADE (Tangent and Adjoint PENultimate Automatic Differentiation Engine) (INRIA 2002) and manual coding. TAPENADE is an automatic code differentiation tool from the Institut National de Recherche en Informatique et en Automatique (INRIA), which is available via the web (http://tapenade.inria.fr:8080/tapenade/index.jsp, August 2006).

RO data and background data

A careful selection and characterization of input data and background fields it necessary to reach a meaningful analysis.

RO observations

The data used in an assimilation system requires some careful considerations to not jeopardize the whole optimization process even if the observations seem to be of high quality.

Choice of used quantity

Observations are used as unprocessed as possible in data assimilation (Kuo et al. 2000), since the characterization of errors becomes increasingly difficult after several processing steps (Rieder and Kirchengast 2001). Attention must be paid to the "incest problem", a phenomenon caused by using background information as well in observation pre-processing steps, resulting in an analysis which is artificially drawn closer to the background than justified. The options for RO data are bending angles or refractivities; we chose refractivity data since it is less demanding in terms of CPU. Assimilating bending angles using a local bending angle operator is considered for future developments, which has the advantage of reduced vertical correlation of the observations (Healy and Thépaut 2006), full 3D ray-tracing is computational not feasible at the moment.

Table 1 Distribution per time layer of the CHAMP occultation data for the test-bed month July 2003

Time layer	Number of profiles	Number of observations (single data points assimilated)
00 UTC	1,193	65,252
06 UTC	1,064	58,603
12 UTC	1,117	60,907
18 UTC	1,165	64,161

RO processing and preprocessing

Observations entering an assimilation framework must be bias free. Within the lower troposphere (<5 km), CHAMP data exhibit a negative refractivity bias of up to 2% and in the Amazons region a positive biases exceeding 1% has been reported (Beyerle et al. 2006), but residual biases in the UTLS region are very small. Since we decided to use data only within 5–35 km, a bias removal procedure is omitted. The CHAMP data had been processed using the WegCenter geometric optics (GO) retrieval scheme (Gobiet et al. 2007). The GO method is an adequate choice for our altitude range of interest whereas in the lower troposphere radio-holographic methods would be preferable.

In general RO data products exceed the vertical resolution of the used model grid by far (300–400 observations within ECMWF model range ~5 to ~35 km), thus data reduction has to be performed prior to assimilation. The purpose is to reduce the numerical cost and to perform a smoothing since the vertical resolution of the observations captures smaller scale atmospheric features than the background grid is capable to do. We dealt with this by aggregating two "super observations" between two vertical model levels, generated by linear averaging in *log* refractivity space. The adequacy of this thinning procedure has been confirmed by sensitivity tests (Löscher 2004).

RO error characteristics

A refractivity error formulation following Steiner and Kirchengast (2005), based on empirically estimated error covariance matrices, was implemented. This approach assumes full vertical correlation within a profile but no horizontal correlation between different profiles since the separation in space and time is sufficient.

Spatial and local time distribution

Homogeneous global coverage is impossible based on a single, near polar orbiting satellite such as CHAMP (more profiles at high latitudes than in the tropics and inhomogeneous local time sampling). For our application we focus on monthly and seasonal means, in line with RO-only climatologies (Foelsche et al. 2007), which is an averaging time frame allowing for sufficient spatial coverage and reasonable local time sampling (Pirscher et al. 2007). July 2003 has been chosen as "test-bed" month to perform a complete test run with the 3D-Var system; Table 1 and Fig. 2 show the characteristics of the respective CHAMP dataset.

Background data

In an operational NWP context the choice of background is naturally limited to the model output our application allows to choose any appropriate fields.

First guess fields

The background data for the test-bed month (July 2003, no RO data assimilated by ECMWF) consisted of temperature, specific humidity, and surface pressure fields from short-range ECMWF forecasts. Since ECMWF assimilates RO data as of Dec 2006 (Healy 2007) and these fields can receive discontinuities from ECMWF operational system changes (e.g. the January–February 2006 discontinuity shown by Borsche et al. (2007) and Steiner et al. (2007)), a more independent background is considered for use in the future (see "Summary and conclusions"). ECMWF runs forecasts twice daily, starting from 00 UTC and 12 UTC; we used 24 h forecasts for the 00 UTC and 12 UTC layers and 30 h forecasts for the 06 UTC and 18 UTC layers, respectively.

Background error characteristics

Prior studies investigated ECMWF analysis global mean error characteristics (M. Fisher, ECMWF, personal communications (2003); Löscher (2004)). This set of standard deviations as function of model levels, and the correlation matrices as function of point separation for the vertical and horizontal dimensions, were taken as the basis for the background error formulation. In our test-bed case we assumed a 50% error growth within 24 h which had been scaled linearly to 30 h. This assumption is somewhat

Fig. 2 Global distribution of
the geo-location of CHAMP RO
profiles for the test-bed month
July 2003
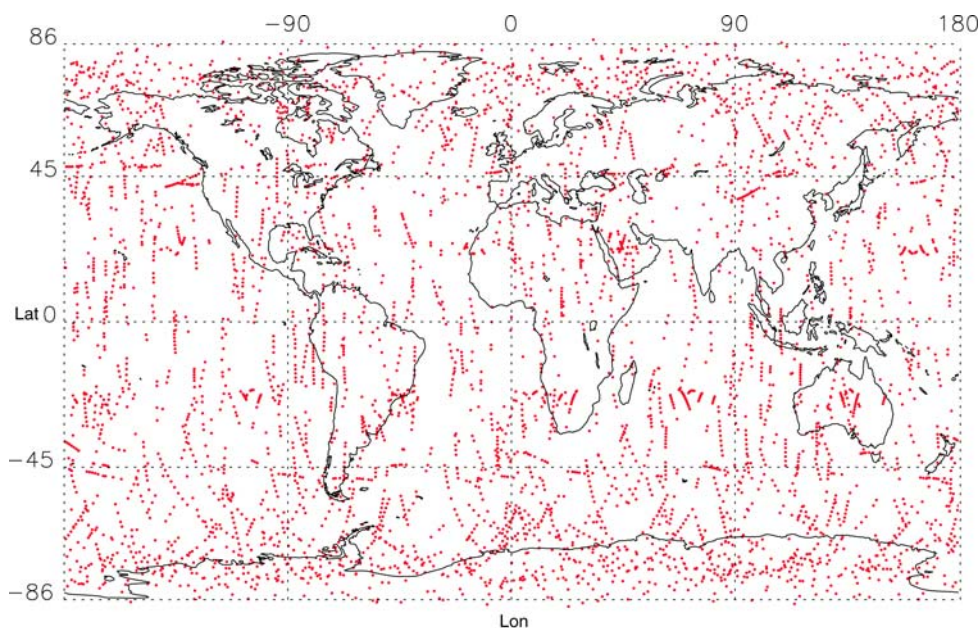
simplistic but appropriate for a test-bed assessment; the results are fairly insensitive to the detailed percentage value ($\pm 15\%$) of the assumed error growth.

Results and discussion

The assimilation results for the test-bed experiment are presented as monthly zonal mean increments ($\delta \mathbf{x}_a$ in Equation (9)) for temperature from model levels 10–40, covering an altitude interval of about 5–37 km. The specific humidity analysis results are omitted here since most water vapor is within the lower troposphere. At the moment we cut off the profiles at 5 km due to bias concerns so there is not much impact. The use of wave optics processed RO data (Gorbunov 2002; Gorbunov and Lauritsen 2004; Jensen et al. 2003) will allow us to lower the cutoff altitude which will result in a more significant humidity impact. For surface pressure, monthly mean increments are presented as a global map.

Figure 3 shows the zonal mean temperature analysis increment, where significant patterns of alternating warm and cold regions are apparent at high latitudes, especially pronounced at the southern hemisphere (Antarctic winter). This pattern agrees to a certain extend with a comparison study of ECMWF analyses and CHAMP RO data, which was based on temperature difference profiles (Gobiet et al. 2005). There the whole summer season JJA of 2003 was studied whereas we analyzed July 2003 only. One difference in our data is a somewhat less pronounced but clearly visible pattern over the northern high latitudes, barely apparent in the other study, which in turn shows a

systematic cold difference at the low latitude tropopause that is not detectable in our results. In general the increments are smaller in our analysis. This difference with respect to Gobiet et al. (2005) can be explained by the fact that the assimilation takes both the background and the observation uncertainties into account.

Regarding other RO data assimilation studies, the results agree fairly well with typical temperature and surface pressure analysis increments, e.g. those in a study on RO impacts at ECMWF by Healy and Thépaut (2006), where observations from August and September 2003 were used. Refractivity differences (not separately shown), calculated from background and analysis data, mirror the temperature increment pattern in Fig. 3 with opposite sign, as expected since refractivity is inversely proportional to temperature (cf. Rieder and Kirchengast 2001; Steiner and Kirchengast 2005).

Figure 4 shows the surface pressure increments, which are small in general but exhibit pronounced features over Antarctica. A similar phenomenon in the analysis increments was observed in the results of Healy and Thépaut (2006). This effect is most likely caused by the orography of the Antarctic plateau. The magnitude of the increments depends on the distance between the surface and the lowermost observation, consistent with Palmer et al. (2000).

Summary and conclusions

We introduced a 3D-Var assimilation scheme for combining GNSS RO data and ECMWF forecast fields for global analyses. The system was end-to-end tested with

Fig. 3 Monthly zonal mean temperature increment field, July 2003
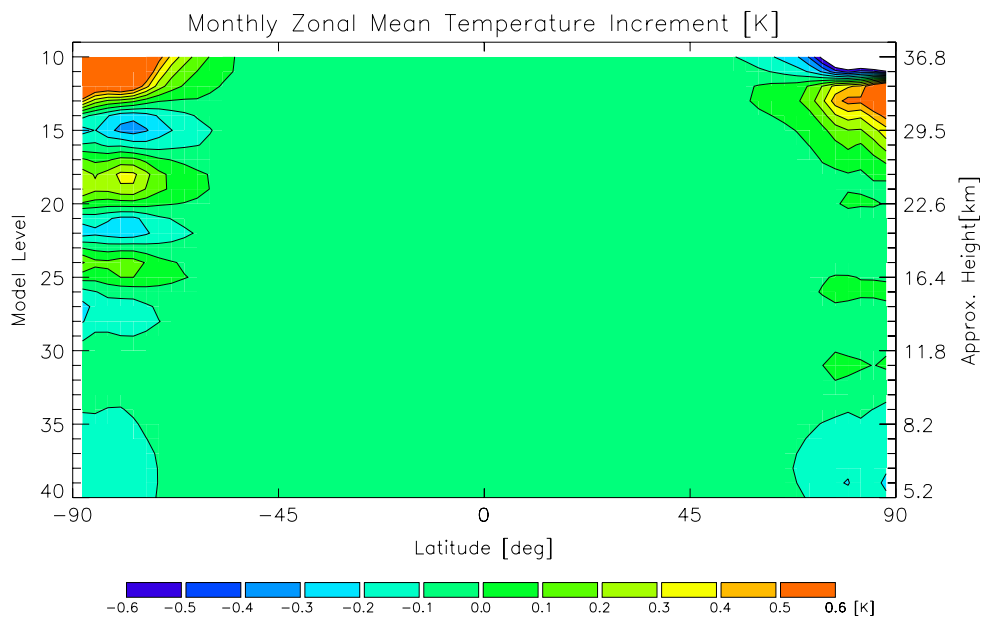
Fig. 4 Monthly zonal mean surface pressure increment field, July 2003
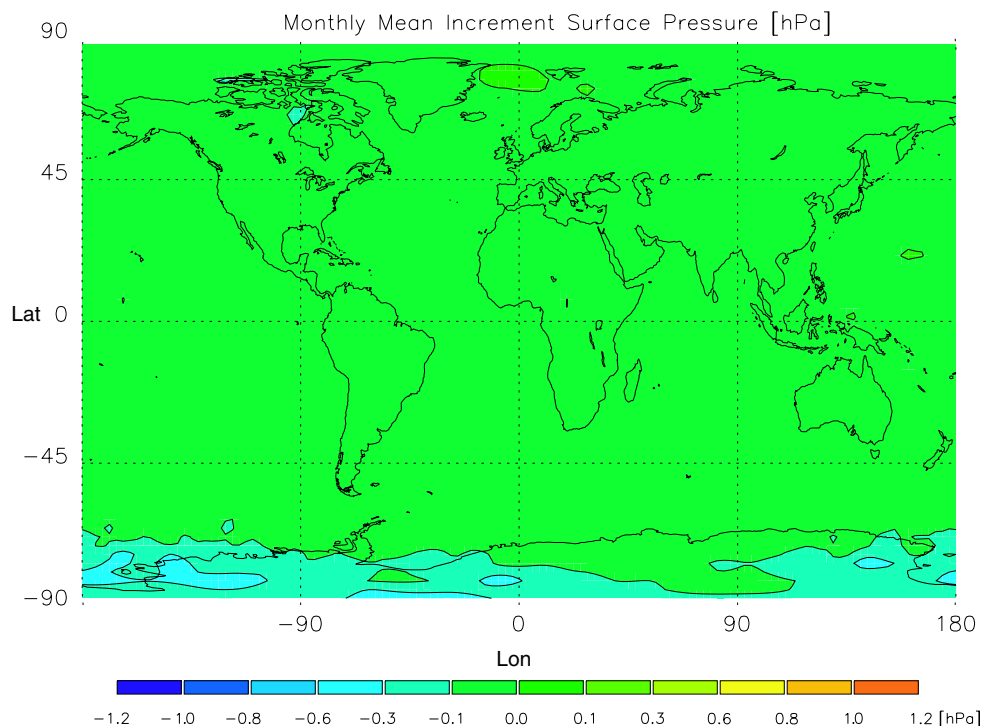
1 month of CHAMP RO data for July 2003. The outcome of this test-bed assessment is encouraging as we find the results consistent with other recent studies (Gobiet et al. 2005; Healy and Thépaut 2006; Foelsche et al. 2007).

Challenges inherent to assimilation systems are correct errors definitions. We are confident concerning the error estimates of the RO data at refractivity level. A bigger challenge is posed by the error structure of the background fields which are currently modeled in a simplistic manner. Taking that fact into account the consistency of the results

is very good, nevertheless the **B** matrix is a backbone of assimilation systems and the definition should be refined (e.g. latitude dependent errors). Based on the test-bed results we conclude that the use of assimilation methods for generating climate analyses is feasible and complementary to RO-only climatologies. The presented results demonstrate a lower-limit baseline for the future impact of RO data. For example, the use of wave-optics retrieval methods will improve the RO retrieval quality especially in the lower to middle troposphere under moist conditions

(tropics), having a favorable impact on the humidity and surface pressure analysis.

In order to be model independent we consider deriving monthly mean background fields from re-analysis data, though reliable error estimates for this kind of fields is a significant effort. From the GNSS RO observation point of view, the complementary implementation of a bending angle operator is considered. Overall the present findings encourage future developments and the promotion of the approach for longer term climatologic analyses, validation of other data sets, and atmospheric variability studies.

References

Anthes RA, Rocken C, Kuo Y (2000) Applications of COSMIC to meteorology and climate. Terr Atmos Ocean Sci 11:115–156

Barker DM, Huang W, Guo Y-R, Bourgeois AJ (2003) A three-dimensional variational data assimilation system for use with MM5. NCAR Tech. Note, NCAR/TN-453 + STR, p 68 [available from UCAR Communications, P.O. Box 3000, Boulder, CO 80307]

Barker DM, Huang W, Guo Y-R, Bourgeois AJ, Xiao QN (2004) A three-dimensional variational data assimilation system for MM5: implementation and initial results. Mon Weather Rev 132:897–914

Bengtsson L, Hagemann S, Hodges KI (2004) Can climate trends be calculated from reanalysis data? J Geophys Res 109:D11111. doi:10.1029/2004JD004536

Beyerle G, Schmidt T, Wickert J, Heise S, Rothacher M, König-Langlo G, Lauritsen KB (2006) Observations and simulations of receiver-induced refractivity biases in GPS radio occultation. J Geophys Res 111:D12101. doi:10.1029/2005JD006673

Borsche M, Kirchengast G, Foelsche U (2007) Tropical tropopause climatology as observed with radio occultation measurements from CHAMP compared to ECMWF and NCEP analyses. Geophys Res Lett 34:L03702. doi:10.1029/2006GL027918

Bouttier F, Courtier P (1999) Data assimilation concepts and methods, meteorological training course lecture series. ECMWF, Reading

Foelsche U, Gobiet A, Steiner AK, Borsche M, Wickert J, Schmidt T, Kirchengast G (2006) Global climatologies based on radio occultation data: the CHAMPCLIM project. In: Foelsche U, Kirchengast G, Steiner AK (eds) Atmosphere and climate, studies by occultation methods, Springer, Berlin, pp 303–314

Foelsche U, Borsche M, Steiner AK, Gobiet A, Pirscher B, Kirchengast G (2007) Observing upper troposphere–lower stratosphere climate with radio occultation data from the CHAMP satellite. Climate Dyn (revised)

Gobiet A, Foelsche U, Steiner AK, Borsche M, Kirchengast G, Wickert J (2005) Climatological validation of stratospheric

temperatures in ECMWF operational analyses with CHAMP radio occultation data. Geophys Res Lett 32:L12806. doi:10.1029/2005GL022617

Gobiet A, Kirchengast G, Manney GL, Borsche M, Retscher C, Stiller G (2007) Retrieval of temperature profiles fro CHAMP for climate monitoring: intercomparison with Envisat MIPAS and GOMOS and different atmospheric analyses. Atmos Chem Phys 7:3519–3536

Gorbunov ME (2002) Canonical transform method for processing radio occultation data in the lower troposphere. Radio Sci 37:1076, doi:10.1029/2000RS002592

Gorbunov ME, Lauritsen KB (2004) Analysis of wave fields by Fourier integral operators and their application for radio occultations. Radio Sci 39:RS4010. doi:10.1029/2003RS002971

Hayden CM, Lorenc AC (1995) Recursive filter for objective analysis of meteorological fields, applications to NESDIS operational processing. J Appl Meteor 34:3–15

Healy SB (2007) Operational assimilation of GPS radio occultation measurements at ECMWF. ECMWF Newsl 111:6–11

Healy SB, Thépaut J-N (2006) Assimilation experiments with CHAMP GPS radio occultation measurements. Q J R Meteorol Soc 132:605–623. doi:10.1256/qj.04.182

Healy SB, Jupp AM, Marquardt C (2005) Forecast impact experiment with GPS radio occultation measurements. Geophys Res Lett 32:L03804. doi:10.1029/2004GL020806

INRIA (2002) Software TAPENADE inria 2002, version 2.0, Tech. Rep. Domaine de Voluceau, Rocquencourt—BP 105, 78153 Le Chesnay Cedex, France

IPCC (2007) Solomon S, Qin D, Manning M, Chen Z, Marquis M, Averyt KB, Tignor M, Miller HL (eds) Climate change 2007—the physical science basis, contribution of WG I to the fourth assessment report of the IPCC. Cambridge University Press, Cambridge and New York, p 996

Jensen AS, Lohmann MS, Benzon H-H, Nielsen AS (2003) Full spectrum inversion of radio occultation signals. Radio Sci 38:1040. doi:10.1029/2002RS002763

Kållberg P, Simmons A, Uppala S, Fuentes M (2004) The ERA40 archive, ERA40 project report series No. 17, ECMWF. Shinfield Park, Reading

Kalnay E (2003) Atmospheric modeling, data assimilation and predictability. Cambridge University Press, Cambridge

Kirchengast G, Steiner AK, Foelsche U, Kornblueh L, Manzini E, Bengtsson L (2000) Spaceborne climate change monitoring by GNSS occultation sensors. In: Proceedings of the 11th symposium on global change studies, Amer Met Soc Annual Meeting 2000, Long Beach, CA, USA, pp 62–65

Kistler R, Kalnay E, Collins W, Saha S, White G, Woollen J, Chelliah M, Ebisuzaki W, Kanamitsu M, Kousky V, van den Dool H, Jenne R, Fiorino M (2001) The NCEP-NCAR 50-year reanalysis: CD-ROM and documentation. Bull Am Meteor Soc 82:247–268

Kozo N (Ed.) (1997) Data assimilation in meteorology and oceanography: theory and practice. Special issue of the J Meteorol Soc Japan 75,1B, Meteorological Society of Japan

Kuo Y-H, Sokolovskiy SV, Anthes RA, Vandenberghe F (2000) Assimilation of GPS radio occultation data for numerical weather prediction. Terr Atmos Ocean Sci 11:157–186

Kursinski ER, Hajj RA, Hardy KR, Schofield JT, Linfield R (1997) Observing the Earth's atmosphere with radio occultation measurements using the global positioning system. J Geophys Res 102:23429–23465

Leroy SS, North GR (2000) The application of COSMIC to global change research. Terr Atmos Ocean Sci 11:187–210

Leroy SS, Anderson JG, Dykema JA (2006) Testing climate models using GPS radio occultation: a sensitivity analysis. J Geophys Res 111: D17105. doi:10.1029/2005JD006145

Löscher A (2004) Assimilation of GNSS radio occultation data into GCM fields for global climate analysis. Wiss Ber 22:211, Institute for Geophysics, Astrophysics, and Meteorology, University of Graz, Austria

Löscher A, Foelsche U, Kirchengast G (2006) CHAMP radio occultation data assimilation into ECMWF fields for global climate analyses. Tech Rep for FFG–ALR 2/2006, Wegener Center, University of Graz, Austria

Loiselet M, Stricker N, Menard Y, Luntama J-P (2000) GRAS—MetOp's GPS-based atmospheric sounder. ESA Bull 102:38–44

Lorenc AC (1992) Analysis methods for numerical weather prediction. Q J R Meteorol Soc 112:1177–1194

Luntama J-P, Kirchengast G, Borsche M, Foelsche U, Steiner AK, Healy S B (2007) EPS GRAS mission for operational radio occultation measurements. Bull Am Meteorol Soc (submitted)

Nocedal J (1996) Large Scale Unconstrained Optimization. Tech Rep Dept of Electrical Engineering and Computer Science, Northwestern University, Evanston/Chicago, IL, USA

Palmer P, Barnett JJ, Eyre JR, Healy SB (2000) A non-linear optimal estimation inverse method for radio occultation measurements of temperature, humidity and surface pressure. J Geophys Res 105:17513–17526

Pirscher B, Foelsche U, Lackner BC, Kirchengast G (2007) Local time influence in single-satellite radio occultation climatologies from Sun-synchronous and non-Sun-synchronous satellites. J Geophys Res 112:D11119. doi:10.1029/2006JD007934

Rieder M J, Kirchengast G (2001) Error analysis and characterization of atmospheric profiles retrieved from GNSS occultation data. J Geophys Res 106:31755–31770

Rocken C, Kuo Y, Schreiner WS, Hunt D, Sokolovskiy S, McCormick C (2000) COSMIC system description. Terr Atmos Ocean Sci 11:21–52

Skamarock WC, Klemp JB, Dudhia J, Gill DO, Barker DM, Wang W, Powers J G (2005) A description of the advanced research WRF Version 2. NCAR/TN-468+STR, NCAR TECHNICAL NOTE, Mesoscale and Microscale Meteorology Division, NCAR Boulder, CO, USA

Steiner A K, Kirchengast G (2005) Error analysis for GNSS radio occultation data based on ensembles of profiles from end-to-end simulations. J Geophys Res 110:D15307. doi:10.1029/2004JD005251

Steiner AK, Kirchengast G, Foelsche U, Kornblueh L, Manzini E, Bengtsson L (2001) GNSS occultation sounding for climate monitoring. Phys Chem Earth A 26:13–124

Steiner AK, Löscher A, Kirchengast G (2006) Error characteristics of refractivity profiles from CHAMP radio occultation data. In: Foelsche U, Kirchengast G, Steiner AK (eds) Atmosphere and climate, studies by occultation methods. Springer, Berlin, 27–36

Steiner AK, Kirchengast G, Borsche M, Foelsche U, Schoengassner T (2007) A multi-year comparison of lower stratospheric temperatures from CHAMP radio occultation data with MSU/AMSU records. J Geophys Res 112. doi:10.1029/2006JD008283 (in press)

Thorne PW, Parker DE, Christy JR, Mears CA (2005) Uncertainties in climate trends: lessons from upper-air temperature records. Bull Am Meteorol Soc 86:1437–1442

Wickert J, Reigber C, Beyerle G, Konig R, Marquardt C, Schmidt T, Grunwaldt L, Galas R, Meehan TK, Melbourne WG, Hocke K (2001) Atmosphere sounding by GPS radio occultation: first results from CHAMP. Geophys Res Lett 28:3263–3266

Wickert J, Schmidt T, Beyerle G, König R, Reigber C, Jakowski N (2004) The radio occultation experiment aboard CHAMP: operational data analysis and validation of vertical atmospheric profiles. J Meteorol Soc Japan 82:381–395

Wu B-H, Chu V, Chen P, King T (2005) FORMOSAT-3/COSMIC science mission update. GPS Solut 9:111–121. doi:10.1007/s10291-005-0140-z

Zhu C, Byrd RH, Lu P, Nocedal J (1995) L_BFGS_B fortran subroutines for large scale bound constrained optimization, L BFGS B_FORTRAN sub routines for large scale bound constrained optimization. Tech Rep Department of Electrical Engineering and Computer Science, Northwestern University, Evanston/Chicago, IL, USA

Zupanski M (1993) A precondition algorithm for large-scale minimization problems. Tellus 45A:478–492

Author Biography

Armin Löscher He received the diploma degree in physics from the Technical University of Graz 2000. He received the PhD degree 2004 from the Department of Geophysics, Astrophysics and Meteorology at the University of Graz. Until 2006 he worked as a visiting scientist for the GRAS Satellite Application Facility at the Danish Meteorological Institute in Copenhagen. Since 2007 he holds a position as research fellow at the European Space Research and Technology Centre (ESA/ESTEC) working on future earth observation missions. His research interests are statistical optimisation, data analysis and advanced concepts in atmospheric remote sensing.